BIOENGINEERING

# Flexible and stretchable nanowire-coated fibers for optoelectronic probing of spinal cord circuits

Chi Lu,[1,2]* Seongjun Park,[2,3]* Thomas J. Richner,[4] Alexander Derry,[1] Imogen Brown,[5] Chong Hou,[1,2] Siyuan Rao,[2] Jeewoo Kang,[6] Chet T. Moritz,[4] Yoel Fink,[1,2,7] Polina Anikeeva[1,2]†



**Studies of neural pathways that contribute to loss and recovery of function following paralyzing spinal cord injury require devices for modulating and recording electrophysiological activity in specific neurons. These devices must be sufficiently flexible to match the low elastic modulus of neural tissue and to withstand repeated strains experienced by the spinal cord during normal movement. We report flexible, stretchable probes consisting of thermally drawn polymer fibers coated with micrometer-thick conductive meshes of silver nanowires. These hybrid probes maintain low optical transmission losses in the visible range and impedance suitable for extracellular recording under strains exceeding those occurring in mammalian spinal cords. Evaluation in freely moving mice confirms the ability of these probes to record endogenous electrophysiological activity in the spinal cord. Simultaneous stimulation and recording is demonstrated in transgenic mice expressing channelrhodopsin 2, where optical excitation evokes electromyographic activity and hindlimb movement correlated to local field potentials measured in the spinal cord.**

## INTRODUCTION

Traumatic injuries to the spinal cord are frequently associated with loss of organ function or loss of voluntary limb control. Our understanding of and ability to treat these symptoms is currently limited by the tools available for monitoring and manipulating neural dynamics within the spinal cord. Because of the relative ease of genetic manipulation, rodent models have become indispensible discovery tools for basic neuroscience. Optogenetic modulation of genetically identifiable neuronal populations in rodent spinal cords may enable discovery of the neural pathways crucial for recovery following injury. However, the spinal cord's viscoelastic modulus of 0.25 to 0.3 MPa (*1*) poses engineering challenges to the design of optoelectrophysiological probes. Furthermore, repeated spinal cord deformations during normal movement demand resilience of the implantable devices to bending and extension fatigue.

Inspired by preclinical (*2*) and early clinical (*3*, *4*) studies indicating the promise of spinal stimulation to facilitate rehabilitation following paralyzing injury, recent work has focused on flexible and stretchable probes for optical and electrical stimulation on the surface of rodent spinal cords (*5*, *6*). The ability to perform neural recording during stimulation may similarly be essential to elucidate the electrophysiological origins of functional recovery. Furthermore, devices suitable for implantation deep within the spinal cord may permit interrogation of specific interneurons, isolating their functional contributions to loss and recovery of connections following injury. Here, we report flexible and stretchable probes that combine optical stimulation with electrophysiological recording that can be implanted into the mouse spinal cord. We adopt a thermal drawing process to produce polymer fibers, and then coat these devices with micrometer-thick meshes of conductive silver nanowires (AgNWs). We characterize electrical impedance and optical transmission of these probes during deformations commonly occurring in rodent spinal cords, thereby illustrating the resilience of the polymer fiber cores and concentric mesh electrodes to strain. Electrophysiological recording of spontaneous, sensory-evoked, and optically evoked neural activity in the spinal cords of mice expressing channelrhodopsin 2 (ChR2) further illustrates the promise of these hybrid fiber probes for studies of spinal cord circuits. Recording of endogenous activity in freely moving mice chronically implanted with fiber probes in their spinal cords, combined with analysis of the surrounding tissue, suggests minimal disruption to local neural networks.

[1]Department of Materials Science and Engineering, Massachusetts Institute of Technology, Cambridge, MA 02139, USA. [2]Research Laboratory of Electronics, Massachusetts Institute of Technology, Cambridge, MA 02139, USA. [3]Department of Electrical Engineering and Computer Science, Massachusetts Institute of Technology, Cambridge, MA 02139, USA. [4]Departments of Rehabilitation Medicine and Physiology and Biophysics, Center for Sensorimotor Neural Engineering, UW Institute for Neuroengineering, University of Washington, Seattle, WA 98195, USA. [5]Department of Materials, University of Oxford, Oxford OX1 3PH, U.K. [6]Department of Chemical Engineering, Massachusetts Institute of Technology, Cambridge, MA 02139, USA. [7]Advanced Functional Fabrics of America Inc., 500 Technology Square, NE47-525, Cambridge, MA 02139, USA.
*These authors contributed equally to this work.
†Corresponding author. Email: anikeeva@mit.edu

## RESULTS

### Design and fabrication of the nanowire-coated fiber probes

To fabricate probes suitable for electrophysiological recording and optical neuromodulation in rodent spinal cords, we combined two techniques. First, we used thermal drawing to produce a flexible optical fiber that also served as a structural core for the probe (Fig. 1A). Being versatile and scalable, thermal drawing can be applied to macroscale templates (preforms) composed of multiple materials. It also allows us to reduce final device dimensions by up to 200 times (fig. S1) while producing hundreds of meters of fiber in a single draw (Fig. 1B) (*7*, *8*). By tuning the stress during the drawing process, a range of feature dimensions can be achieved without compromising the cross-sectional geometry defined within the preform (fig. S1).

On the basis of previous work applying multimaterial fibers to optical neuromodulation (*9*, *10*), polycarbonate (PC; refractive index $n$ = 1.58; glass transition temperature $T_g$ = 145°C; Young's modulus $E$ = 2.38 GPa) and cyclic olefin copolymer (COC; $n$ = 1.52, $T_g$ = 158°C, $E$ = 3.0 GPa) were selected as the respective core and cladding of the optical fiber (*11*–*13*). To enable neural recording while minimizing the device footprint, we deposited uniform 1-μm-thick conductive layers of AgNWs (diameter $d$ = 70 nm; length $L$ = 40 μm) (Fig. 1, A and C) over the COC cladding via dip coating from isopropanol (IPA) solutions with different concentrations (Fig. 1, A, D to F). Because the hydrophobicity of COC limited the adhesion and deposition

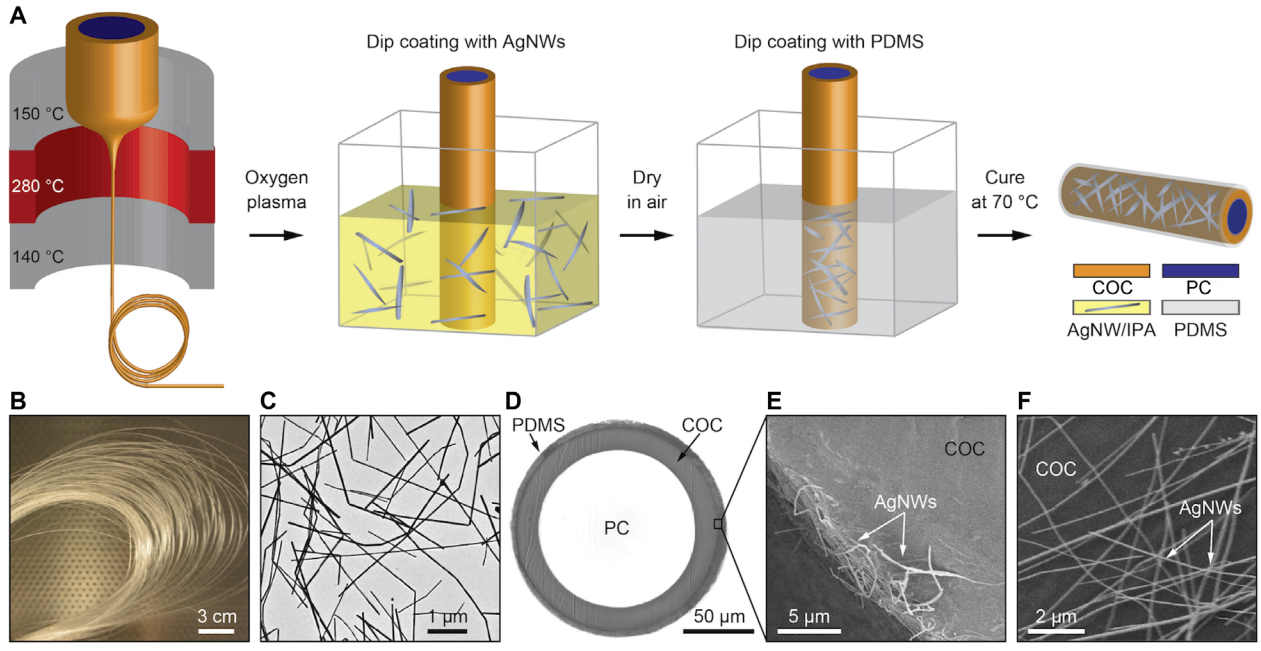


**Fig. 1. Fabrication of flexible neural probes.** (**A**) Illustration of the fiber probe fabrication. (**B**) Spool of a fiber with PC core and COC cladding. (**C**) Transmission electron microscopy (TEM) image of the AgNWs. (**D**) Cross-sectional image of the fiber probe. (**E**) Scanning electron microscopy image shows a portion of the ring AgNW electrode cross section. (**F**) Scanning electron microscopy image of the AgNW mesh on top of the fiber surface.

of AgNWs from IPA (*14*), oxygen plasma treatment of the fibers was essential to enhance the uniformity of AgNW mesh layers (*14*, *15*). An AgNW coating was chosen as the electrode material because of its high conductivity and compatibility with facile solution-based processing (*16*). It was hypothesized that the mesh formed by AgNWs would be more resilient with respect to bending and stretching deformation (*17*, *18*) than a continuous metallic film of comparable thickness, because the latter is anticipated to develop cracks under strains commonly experienced in spinal cords (*19*). The entire structure was then encapsulated within a layer of polydimethylsiloxane (PDMS; $n$ = ~1.41 to 1.47; thickness, 5 μm) (*20*) to minimize direct contact of AgNW with tissue and prevent surface oxidation and mechanical degradation (Fig. 1, A and D). The final device diameter ranged from 105 to 135 μm and was constrained by the dimensions of the structural fiber core (100 to 130 μm).

## Optical and electrical properties of the nanowire-coated fiber probes

To match the mechanical properties of neural tissues, flexible polymer-based optical waveguides have been recently introduced to replace conventional rigid silica fibers (*21*–*27*). Waveguides composed of SU-8 and poly(methyl methacrylate) (PMMA) fabricated via a lithographic process have been used in the context of optogenetic neuromodulation (*23*), whereas PDMS and hydrogel-based devices have been applied to fluorescence measurements and optical control of gene expression (*20*, *26*, *27*). In addition to their transparency across the visible spectrum (fig. S2), the polymers PC and COC are compatible with the thermal drawing process. Consequently, the geometry of the device can be easily altered to fit the application (*28*). The difference between the refractive indices of PC and PDMS is 0.18. Although this should, in principle, be sufficient to sustain multimode transmission through the fiber even in the absence of COC cladding (fig. S2), direct coating of AgNWs onto the PC surface resulted in significant losses due to scattering and evanescent coupling of light into the plasmon modes of these nanomaterials (Fig. 2A) (*29*). Addition of the COC cladding reduced the losses from 2.5 to 1.9 dB/cm (Fig. 2A). Because of their flexibility, these probes were able to maintain transmission under extreme deformations (Fig. 2B), including their use as sutures (Fig. 2C).

Electrophysiological recording during optogenetic neuromodulation is commonly accomplished by integrating conductive electrodes within the probes (*23*, *30*–*34*). Conductive polymer composites exhibit high flexibility and biocompatibility (*35*), but are limited by high impedances on the order of megohms (*9*, *10*, *36*). Metallic electrodes deposited on polymer substrates have low impedance but are subject to cracking (*19*). Fractal and serpentine metallic electrodes defined via contact printing address the flexibility challenge but offer limited spatial resolution (*5*, *6*, *37*–*39*). AgNW meshes were previously used as stretchable interconnects in flexible electronic applications (*16*), and their composites have been recently applied to monitoring of cardiac function (*35*). We found that to reproducibly achieve meshes with low resistivity, the concentration of AgNWs in a dip-coating solution needed to exceed 4 mg/ml. At concentrations >6 mg/ml, the resistivity of the AgNW mesh was proportional to the concentration of the dip-coating solution (Fig. 3A). To account for anticipated changes in mesh morphology during deformation, we chose the lowest resistance mesh ($9.37 \times 10^{-4}$ ohm·cm) for our probes. PDMS was selected as a protective coating for the conductive layer because of its low modulus (tens of kPa for 30:1 polymer to curing agent by weight) and low refractive index, ensuring confinement of light to the PC/COC core (*40*). Following dip coating with PDMS, the probe tips were cut orthogonally to the fiber axis, exposing thin conductive AgNW ring electrodes. Similar to solid metallic electrodes, the impedance of the probes at 1 kHz had a significant dependence on the contact area but less on the

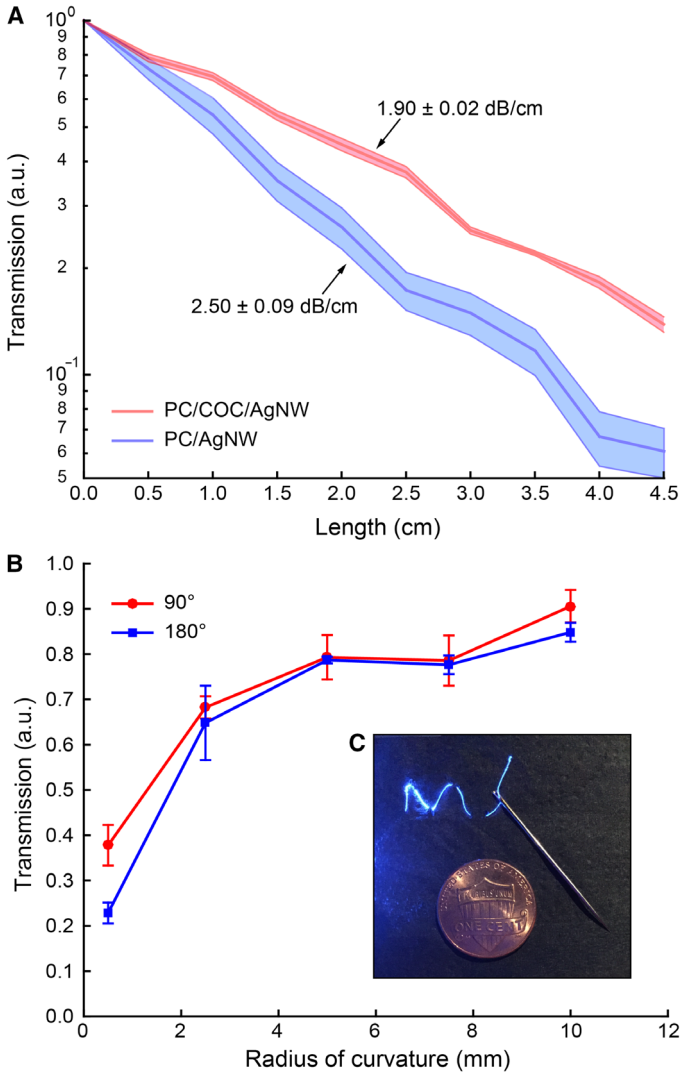


**Fig. 2. Optical characterization of flexible neural probes.** (**A**) Normalized transmission at a wavelength λ = 473 nm as a function of length for fiber probes with and without COC cladding to separate AgNW mesh from the PC optical core with a diameter of 120 μm. (**B**) Transmission at λ = 473 nm for PC/COC/AgNW/PDMS fiber probes (core diameter, 120 μm) bent at 90° or 180° as radii of curvature (0.5 to 10 mm) displayed relative to straight probes. All scale bars and shaded areas represent SEM. *n* = 5 samples for each data point. (**C**) Image of a PC/COC/AgNW/PDMS fiber probe connected to a laser source, threaded through a needle, and used to create several stitches on fabric.

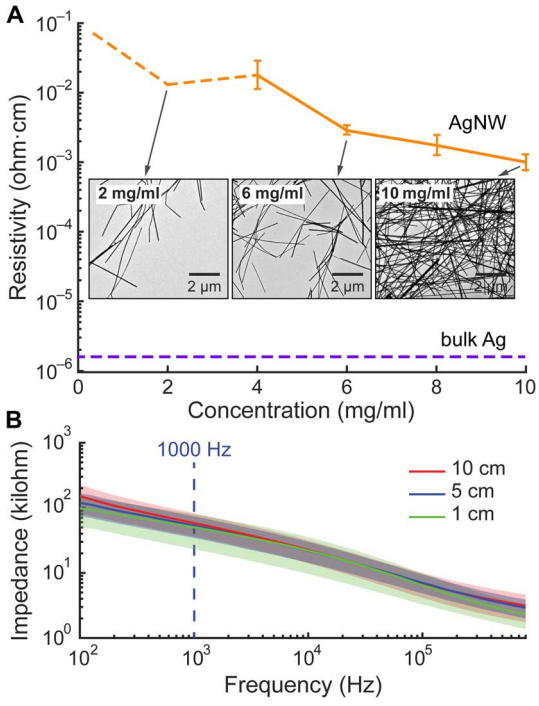


**Fig. 3. Electrical characterization of flexible neural probes.** (**A**) Resistivity of the mesh as a function of AgNW solution concentration. Inset: TEM images of the AgNW meshes deposited from solutions with 2, 6, and 10 mg/ml concentrations. AgNW mesh deposited from the 10 mg/ml solution was used for further characterization and in vivo evaluation. (**B**) Impedance spectra of the AgNW mesh electrodes deposited on 1-, 5-, and 10-cm-long fibers with 120-μm PC/COC cores. All scale bars and shaded regions represent SEM. *n* = 5 samples for each data point.

length. Mesh electrodes within 1- and 10-cm fiber probes exhibited impedance values of similar orders of magnitude ($|Z_{PC/COC,\,1\,cm}|$ = 50 ± 26 kΩ, $|Z_{PC/COC,\,10\,cm}|$ = 58 ± 21 kΩ; mean ± SEM), which indicated that, following evaluation in small rodents, this fabrication approach may, in principle, be scaled to applications in larger animals (Fig. 3B).

In addition to bending, AgNW mesh concentric electrodes were also resilient to stretching deformation. Using a fabrication process identical to the one outlined for PC/COC fibers, we thermally drew stretchable fibers composed of COC elastomer (COCE; *n* = 1.51; melting temperature $T_m$ = 84°C; *E* = 34 MPa). We chose COCE because of its low modulus and compatibility with a range of drawing parameters. To establish stable processing conditions, we introduced sacrificial PMMA cladding into the preform and then removed it with acetone following drawing (Fig. 4). The resulting pillow-shaped COCE fibers (cross-section width × height in the range from 125 μm × 100 μm$^2$ to 250 μm × 200 μm$^2$) were similarly treated with oxygen plasma, dip-coated with AgNWs, and encapsulated with PDMS. Consistent with lower optical transmission of COCE as compared to PC and COC, higher optical losses of 3.98 dB/cm were measured for AgNW-coated COCE core fibers (fig. S3).

Because COCE is a rubbery material, these fibers could sustain up to 230% strain, which was reduced to 200% following the coating with AgNWs and PDMS (Fig. 4A). AgNW mesh electrodes coated onto 1- and 10-cm COCE fibers exhibited somewhat greater difference in impedance ($|Z_{COCE,\,1\,cm}|$ = 34 ± 17 kΩ, $|Z_{COCE,\,10\,cm}|$ = 162 ± 50 kΩ; mean ± SEM; Fig. 4B), as compared to their PC/COC analogs. However, the absolute values of impedance were still well within the range suitable for extracellular recordings even for 10-cm-long fibers.

We found that a single-layer AgNW mesh coating could only withstand strains of ~30% before losing conductivity due to the disruption of the conductive network (fig. S4). In contrast, electrodes composed of a three-layer AgNW mesh maintained low impedance at strains up to ~100% (Fig. 4C). This is consistent with scanning electron microscopy images that do not reveal any structural differences between the AgNW mesh–coated fibers subjected to 0, 10, and 20% strain (Fig. 4D). Repeated extension of the COCE/AgNW/PDMS fibers resulted in negligible hysteresis of the electrode impedance, indicating resilience of these devices to deformation (Fig. 4E). Because the spinal

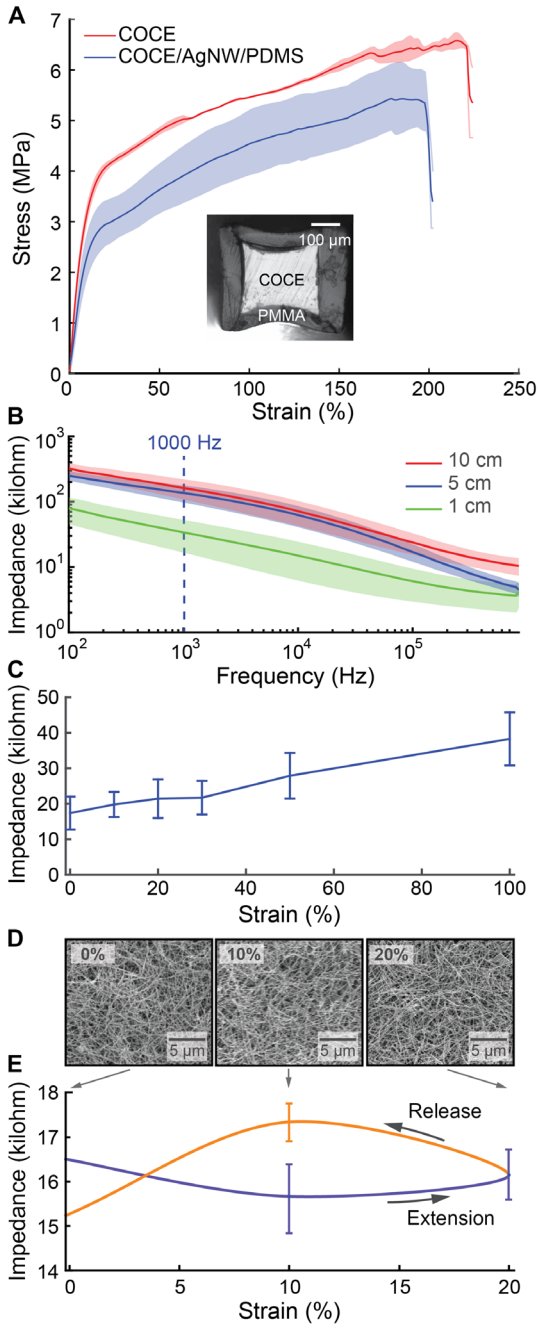


**Fig. 4. Mechanical and electrical characterization of stretchable neural probes.** (**A**) Tensile tests performed for a thermally drawn COCE fiber and a COCE fiber probe coated with three layers of AgNW mesh and a protective PDMS cladding (COCE/AgNW/PDMS) ($n$ = 5 devices). (**B**) Impedance spectra of the AgNW mesh electrodes deposited onto 200 × 200 $\mu m^2$ COCE core fiber with lengths of 1, 5, and 10 cm. (**C**) Impedance of a three-layer AgNW mesh within COCE/AgNW/PDMS probes with core dimensions of 200 × 200 $\mu m^2$ as a function of tensile strain. (**D**) Scanning electron microscopy images of the three-layer AgNW mesh deposited onto COCE fiber at 0, 10, and 20% strain. (**E**) Impedance of fiber probes characterized in (C) measured over five extension and release cycles. All scale bars represent SEM. $n$ = 5 samples for each data point.

cord and peripheral nerves only experience strains up to ~12% (*41*), the low-impedance AgNW mesh–coated fibers provide arbitrarily scalable and stretchable alternatives to polymer composite and metallic electrodes.

### In vivo electrophysiological recording and optical stimulation with nanowire-coated fibers

We evaluated the ability of the AgNW-coated fibers to record and optically stimulate neural activity in the mouse spinal cord (Fig. 5, A and B). Optoelectronic fibers with PC/COC and COCE optical cores were implanted into the lumbar region (L1) of the spinal cord of WT and Thy1-ChR2-YFP transgenic mice that broadly express light-sensitive cation channel ChR2 (*42*). Acute experiments in anesthetized mice indicated the ability of both PC/COC and COCE fiber probes with AgNW electrodes to record spontaneous neural activity (Fig. 5, C to F, and fig. S5). Single-neuron signals were isolated (Fig. 5, D and F) and assessed by principal components analysis (fig. S5, A and C) and interspike interval (ISI) histograms (fig. S5, B and D).

Electrophysiological activity was also recorded with AgNW electrodes within PC/COC- and COCE-based fiber probes in tethered, freely moving WT mice up to 1 week following the implantation surgery (fig. S6). Recordings from freely moving mice contained a combination of multiunit activity and movement artifacts and were confounded by greater noise levels than those performed under anesthesia. However, the noise level remained stable over these week-long studies. In addition to spontaneous activity, we recorded robust sensory-evoked potentials from the dorsal columns that scaled with current applied to the ipsilateral hind foot (Fig. 5, G and H, and fig. S7, A and B).

In Thy1-ChR2-YFP mice, illuminating the lumbar region of the spinal cord with laser light (125 to 168 $mW/mm^2$) with a wavelength $\lambda$ = 473 nm (activation peak of ChR2), coupled into fiber cores through ferrules, consistently evoked neural activity that was correlated with the 5-ms optical pulses at 10 Hz (latency, 10.6 ± 0.5 ms) (Fig. 5, I and J). Stimulation at a higher frequency of 100 Hz similarly evoked neural activity (fig. S8). However, in this case, the observed multineuron potentials did not follow each laser pulse, consistent with ChR2 kinetics (*43*). Neural activity in the lumbar spinal cord induced by optical pulses delivered through the fiber probes was sufficient to produce muscle contractions in the ipsilateral hindlimb (Fig. 5, K and M, fig. S9, and video S1). The electromyographic (EMG) activity recorded in a gastrocnemius muscle (Fig. 5M) was correlated with the optically evoked local field potentials recorded with the AgNW mesh–coated COCE fibers in the lumbar spinal cord (Fig. 5L).

Immunohistochemical analysis of the spinal cord tissue surrounding the fiber probes indicated modest astrocytic presence, as indicated by staining with antibodies against glial fibrillary acidic protein (GFAP), for the devices positioned on the surfaces and within the tissue 2 weeks after the implantation surgeries (fig. S10). Furthermore, the depth probes reaching into the gray matter did not appear to interfere with the viability of the surrounding neuronal populations (fig. S10, D and E).

## DISCUSSION

By combining thermally drawn polymer fibers with solution-deposited nanowires, we developed flexible and stretchable concentric probes suitable for optical and electrophysiological interrogation of spinal cord circuits in the mouse model. Our devices maintained optical and electrical properties under bending and stretching deformations, exceeding those experienced by the mouse spinal cord during normal motion. The mechanical, optical, and electrical characteristics of the probes enabled acute recordings of spontaneous neural activity, sensory-evoked potentials, and the simultaneous recording of optically evoked spinal

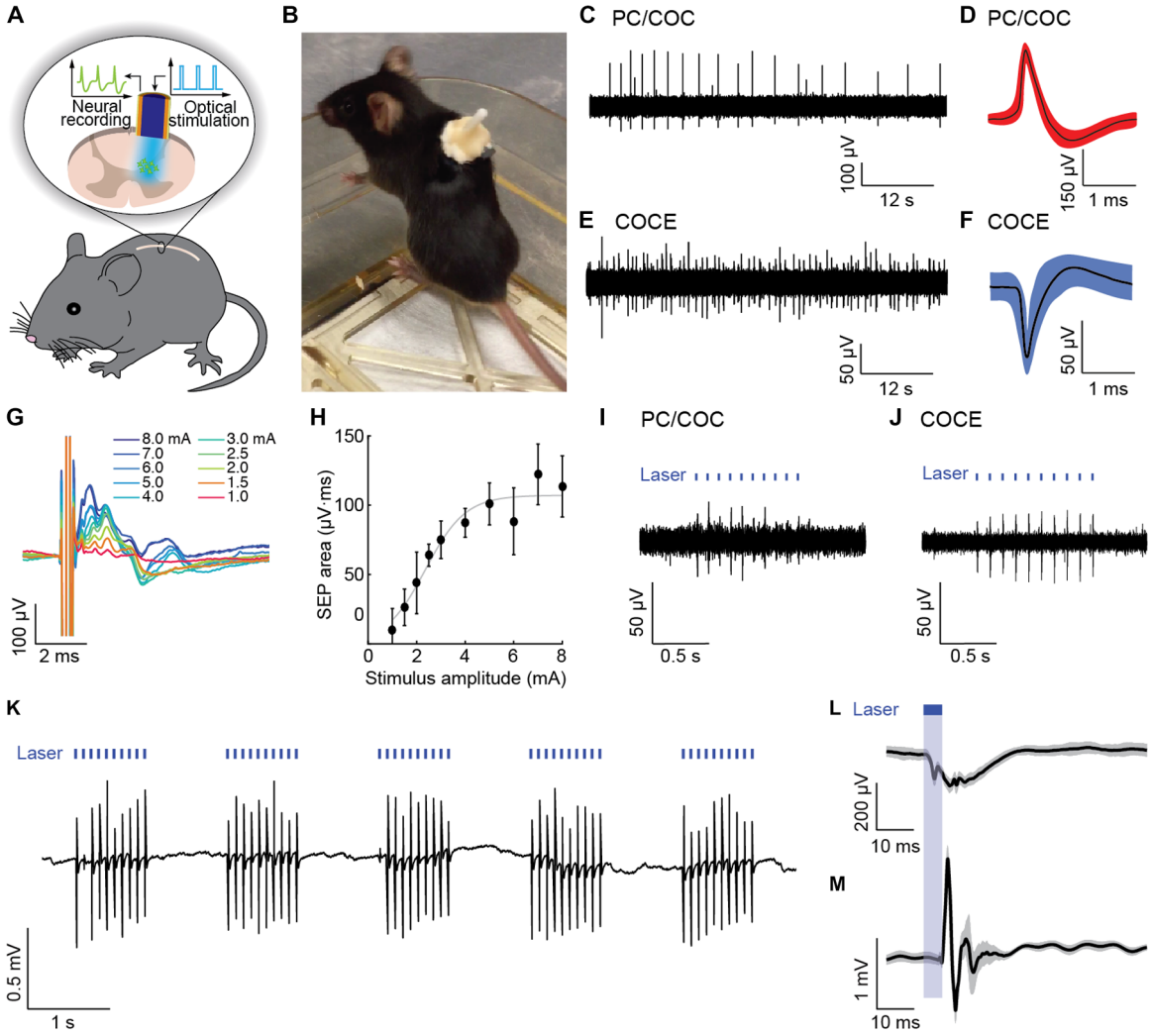


**Fig. 5. Probing spinal cord electrophysiology with flexible and stretchable neural probes.** (**A**) Schematic depicting optical stimulation and electrophysiological recording with a fiber probe in a mouse spinal cord. (**B**) Image of mouse implanted with a flexible neural probe between L1 and L2 exploring its environment. (**C**) Spontaneous activity recorded in acute conditions with AgNW concentric mesh electrodes deposited onto PC/COC core fibers in spinal cord of wild-type (WT) mice. (**D**) Action potentials isolated from the recording in (C). (**E**) Spontaneous activity recorded in acute conditions with AgNW concentric mesh electrodes deposited onto COCE core fibers. (**F**) Action potentials isolated from the recording in (E). (**G**) Sensory-evoked potentials recorded acutely from the dorsal column with AgNW mesh electrodes within PC/COC-based probes at different input currents (1 to 8 mA; 125 µs per phase biphasic). Sensory potentials are preceded by the electrical stimulus artifact. (**H**) Sensory-evoked potential (SEP) recruitment curve relating the area under the first positive peak to the stimulus amplitude. (**I**) Neural activity in a spinal cord of a Thy1-ChR2-YFP mouse evoked by optical stimulation (wavelength $\lambda$ = 473 nm, 168 mW/mm$^2$, 5-ms pulse width, 10 Hz) delivered through the PC/COC fiber and recorded with the concentric AgNW mesh electrodes. (**J**) Neural activity in spinal cord of a Thy1-ChR2-YFP mouse evoked by optical stimulation (wavelength $\lambda$ = 473 nm, 125 mW/mm$^2$, 5-ms pulse width, 10 Hz) delivered through the COCE fiber and recorded with the concentric AgNW mesh electrodes. (**K**) EMG evoked by the optical stimulation in (J). (**L**) Optically evoked local field potentials recorded with AgNW mesh electrodes within COCE fiber. (**M**) An expanded view of the averaged EMG signal from (K).

potentials and optical control of hindlimb muscles. These findings suggest that the fiber platform may, in the future, permit monitoring and controlling of neural activity to promote recovery following spinal cord injury. Isolating single-neuron action potentials from the mouse spinal cord during free behavior remains a goal because such recordings are exceedingly difficult, having been rarely reported in rodents (*44*). Even in acute studies, the flexibility of our probes may provide a solution to the challenges associated with the recording of neural activity in the spinal cord posed by the respiration and heartbeat, which often necessitate a transection of nerves leading to the diaphragm (*45*).

Our conceptual experiments conducted with AgNW meshes as electrodes within fiber probes do not reveal tissue erosion or cytotoxic effects in the vicinity of the implants (fig. S9). These nanomaterials were chosen as an affordable alternative to gold NWs. Going forward, any metallic NWs can be similarly deposited onto polymer fiber surfaces, further enhancing long-term biocompatibility and tunability of charge-carrying capacity (*46*). Additional chemical stability can be achieved through covalent cross-linking of the mesh (*47*), and the surface of the exposed NW ring can be passivated through electrodeposition of gold or iridium oxide layers via established protocols routinely applied to nickel-chromium (Ni/Cr) tetrodes (*48*).

AgNW mesh electrodes enabled straightforward integration of electrophysiological recording capability into polymer optical fibers without significant increase in overall device dimensions. In the future,

the number of channels can be expanded by integrating multiple concentric NW rings separated by thin elastomer coatings and by patterning the mesh electrode surfaces, for example, through the use of photosensitive PDMS (*49*, *50*). The high surface area of exposed NWs, as compared to monolithic electrodes of similar cross section, may permit maintaining impedance values in the range applicable for extracellular recordings, even following patterning of the meshes. The probes demonstrated here relied solely on scalable fiber drawing and solution-based fabrication methods that do not pose constraints on device dimensions or geometry. Acting as flexible and stretchable optical canvases for electrophysiological probes, these fibers may, in the future, be tailored to address fundamental questions in spinal cord or visceral organ neurophysiology.

## MATERIALS AND METHODS

### Fiber probe fabrication

#### *PC/COC waveguide.*

To fabricate a preform, we wrapped a PC cylinder (diameter, 9 mm; McMaster-Carr) in COC sheets (thickness, 0.05 mm; TOPAS Advanced Polymers, 6015S) to the total preform diameter of 12.5 mm. The entire structure was then consolidated at 190°C for 12 min in vacuum. The fiber was drawn at 280°C, and the drawing speed was varied from 1 to 7 m/min to achieve draw-down ratios in the range of 30 to 140.

#### *COCE rubbery fiber.*

To fabricate the preform, we first cast-molded pellets of COCE (TOPAS Elastomer E-140) into rectangular strips ($L$ = 100 mm, $W$ = 6 mm, $H$ = 6 mm) at 180°C in vacuum. PMMA (thickness, 12.7 mm; McMaster-Carr) plates were machined into 25.4 mm-wide strips, followed by machining grooves in the center of each strip and filling those with molded COCE. The preform was then consolidated under pressure (50 psi at 125°C) for 14 hours and cooled to room temperature while concomitantly reducing the applied stress. The preform was drawn at 240°C, and the resulting fiber dimensions were reduced 40 to 80 times.

The fiber probes were connected to zirconia ferrules (Thorlabs, CF128) using optical epoxy (Thorlabs, F112). The ferrule ends of the fibers were then polished with silicon-carbide sandpaper.

### Electrode fabrication and connection

The surface of the fiber probe was treated with oxygen plasma, dipped into IPA solution of AgNWs (10 mg/ml, Novarials NovaWire-Ag-A70-IPA), and dried in the air for at least 3 hours. Copper wire (AWG-38) was placed on the fiber surface, attached with a conductive silver paint (SPI Supplies, 04998AB), and then dried in the air for 2 hours. The AgNW-coated fibers were dipped into PDMS (Sylgard 184, Dow Corning; 30:1 polymer to curing agent by weight) and cured at 70°C for 1 hour. The joint between the fiber probe and the copper wire was sealed with epoxy (Devcon, 5 Minute Epoxy) to enforce the connection. The copper electrode lead was then connected to a four-pin connector (Digi-Key ED90528-ND) for electrophysiological data acquisition. Before implantation, the fiber probes were coated with molten poly(ethylene glycol) (molecular weight, 1000) to temporarily stiffen them for implantation.

### Fiber probe characterization

Optical loss coefficients (in dB/cm) were measured by connecting fiber probes of different lengths to a fiber-coupled 473-nm blue laser (Laserglow Technologies) via ferrule-to-ferrule connection with zirconia sleeves (Thorlabs, ADAF1) and by collecting the power output with a calibrated silicon photodiode (Thorlabs, S121C and PM100D).

Tip impedances of AgNW electrodes were measured in saline solution (0.9 wt %) with an LCR meter (Agilent 4284A) (10 mV) in a frequency range of 0.1 to 1000 kHz. Tensile tests were performed using a nano tensile tester (MTS Nano Instrument UTM390).

### Structural and surface analysis with microscopy

Scanning electron microscopy images were collected using a Zeiss Ultra-55 microscope (4 kV). TEM was performed on a FEI Tecnai G2 Spirit TWIN (120 kV). Optical images were obtained using Zeiss Axioskop 2 MAT microscope with ×10 magnification.

### In vivo studies

All procedures involving vertebrate animals were approved by the Massachusetts Institute of Technology (MIT) Committee on Animal Care. No additional ethical guidelines were considered. Fiber probes were evaluated in male Thy1-ChR2-YFP transgenic (donated by G. Feng) and WT (BL6/57, The Jackson Laboratory) mice housed at the MIT central animal facility (12-hour light/dark cycle at 22°C with food and water ad libitum).

### Fiber implantation

The AgNW- and PDMS-coated PC/COC and COCE fiber probes were acutely and chronically implanted into the lumbar region of the spinal cord of Thy1-ChR2-YFP and WT mice. The mice were anesthetized using isoflurane (5% induction followed by 1.75 to 2.0% in oxygen). Supplemental heat was provided during the surgery. The fur was removed over the dorsum, and the skin was cleaned with alcohol and povidone iodine. One midline incision was made over vertebral segments T13, L1, and L2. The paraspinal muscles were removed to expose the vertebrae. Lateral spinal clamps were used to hold L1 in a stereotaxic frame (Kopf, model 980). The spinal cord was exposed between L1 and L2 by further dissection. The neural probe was placed on the surface of the dorsal side of spinal cord and then lowered by 300 μm into the spinal cord. For chronic implantation, the three segments were fused with dental cement (Metabond, Parkell). This step was omitted during acute experiments. The probes were connected to the neural recording headstage and the optical patch cord (details below) and then lowered into the spinal cord using a stereotaxic manipulator. A low-impedance ground/reference wire (stainless steel) was coiled and placed next to the vertebral column. For chronic implantation, gelfoam was deposited around the probe tips, and the probes were secured with dental cement to the three fused vertebral segments. The mice were dosed with slow-release buprenorphine analgesia and recovered on a warm pad.

### Optical stimulation

Laser pulses were applied through the COCE and PC/COC fiber cores to the spinal cord. A blue laser (diode-pumped solid-state; 473 nm, 100 mW; Laserglow) was coupled to a fiber patch cord [diameter, 50 μm; numerical aperture (NA), 0.22; silica; Thorlabs] with a custom two-mirror setup on an optical breadboard. The patch fiber was coupled to a fiber probe using a ferrule-to-ferrule ceramic sleeve. The laser was controlled by the neural recording setup (Tucker-Davis Technologies, RZ5D) to produce pulse trains of 1-s duration with 5-ms pulses applied at 10 or 100 Hz. Optical power of 2.5 mW was measured at the probe tip, leading to a power density of 125 to 168 mW/mm$^2$ at the surface of the spinal cord.

### Electrophysiological recordings in the spinal cord

Spontaneous and stimulus-evoked potentials were recorded using AgNW mesh electrodes within the PC/COC- and COCE-based probes. The mesh electrodes were connected to a high-impedance headstage (Tucker-Davis Technologies, ZIF-Clip 32) through a custom PCB adapter board. The signals were sampled at 48 kHz (PZ2, Tucker Davis Technologies) and filtered (0.3 to 10 kHz; third-order infinite impulse response) in Matlab (MathWorks). Single-neuron action potentials (spikes) were isolated by detecting threshold crossings at 2 SDs from the noise level, projecting the spikes onto the first two principal components, and then clustering with *k*-means. ISI histograms were calculated from the sorted units.

### Electromyography

EMG signals were recorded from the gastrocnemius muscle with two polytetrafluoroethylene-coated stainless steel wires [A-M Systems; diameter, 50 μm/115 μm (bare/coated)]. The 1-mm tips of the wires were exposed using a scalpel to reduce impedance before insertion into the muscle belly with a 25-gauge needle. The EMG signals were amplified by the high-impedance headstage and sampled at 48 kHz. Single-ended recordings relative to a low-impedance distant reference and ground were collected from each electrode. These recordings were low pass–filtered (25th-order finite impulse response; 5-kHz corner frequency) and subtracted in Matlab to produce a differential recording.

### Sensory-evoked potentials

Sensory-evoked potentials were recorded from the dorsal columns of anesthetized WT mice using AgNW mesh electrodes on PC/COC cores. Electrical stimuli were applied peripherally to the ipsilateral hindlimb. Two stainless steel wires, identical to those described in the EMG section above, were inserted subcutaneously near the ankle. One wire was placed medial to the ankle, and one wire was placed lateral. Biphasic current pulses (125 μs per phase, 1 to 8 mA) were delivered every 2 s. The resulting volley of activity was recorded at the dorsal columns with the AgNW electrodes. The experiment was repeated after flipping the polarity of the biphasic pulse as a control. An adaptive filter was applied to remove power-line noise without introducing impulse response artifacts near the stimulus. The area under the first positive peak was integrated at each stimulus level to create a recruitment curve. The curve was fit to a sigmoid using a weighted least-squares regression on a positive range (Matlab).

### Immunohistochemistry

Long-term tissue responses to the fiber probes implanted over and within the spinal cords were investigated by immunohistochemistry. Two weeks after implantation with PC/COC/AgNW/PDMS or COCE/AgNW/PDMS probes, WT mice ($n$ = 3 per device) were anesthetized via intraperitoneal injection of Fatal-Plus solution (100 mg/kg in saline) and perfused with 4% paraformaldehyde (PFA) in phosphate-buffered saline (PBS). Spinal cords were extracted and fixed in 4% PFA overnight, and then sliced into 50-μm coronal sections using a vibrating blade microtome (Leica VT1000S). Sections were permeabilized and blocked in 0.3% (v/v) Triton X-100 and 3% (v/v) donkey serum in PBS for 30 min. This was followed by overnight incubation at 4°C in a solution of primary antibodies (goat anti-GFAP, 1:1000; rabbit anti-NeuN, 1:500; Fisher Scientific) and 3% donkey serum in PBS. Following incubation, the sections were washed three times for 30 min each with PBS. The slices were then incubated with secondary antibodies (Alexa Fluor 488 donkey anti-goat, 1:1000; Alexa Fluor 633 donkey anti-rabbit, 1:1000; Life Technologies) for 1 hour at room temperature. Following three more washes with PBS, slices were mounted using PVA-DABCO (Sigma-Aldrich) onto glass microscope slides. A laser-scanning confocal microscope (FluoView FV1000, Olympus) with 10× (air, NA = 0.16) objective was used for image acquisition.

## SUPPLEMENTARY MATERIALS

Supplementary material for this article is available at http://advances.sciencemag.org/cgi/content/full/3/3/e1600955/DC1

fig. S1. Controlled parameters during the drawing of the PC/COC fiber.
fig. S2. Optical transmission spectra of PC/COC fibers at visible wavelengths.
fig. S3. Transmission at a wavelength λ = 473 nm for COCE fiber.
fig. S4. Impedance of COCE fibers coated with a single layer of AgNW mesh and measured at 0, 10, and 20% extension strain.
fig. S5. Spontaneous single units isolated during acute anesthetized recordings (see Fig. 5, C to F).
fig. S6. Electrophysiological recording collected from the freely moving mice implanted with fiber probes.
fig. S7. Additional in vivo sensory and electromyographic recordings.
fig. S8. Electrophysiological recordings of optically stimulated activity.
fig. S9. In vivo EMG recordings.
fig. S10. Immunohistochemical analysis of the dorsal horn 2 weeks after device implantation surgeries.
video S1. Optical spinal control of muscle activity.

## REFERENCES AND NOTES


1. S. Cheng, E. C. Clarke, L. E. Bilston, Rheological properties of the tissues of the central nervous system: A review. *Med. Eng. Phys.* **30**, 1318–1337 (2008).
2. I. Lavrov, G. Courtine, C. J. Dy, R. van den Brand, A. J. Fong, Y. Gerasimenko, H. Zhong, R. R. Roy, V. R. Edgerton, Facilitation of stepping with epidural stimulation in spinal rats: Role of sensory input. *J. Neurosci.* **28**, 7774–7780 (2008).
3. V. R. Edgerton, S. Harkema, Epidural stimulation of the spinal cord in spinal cord injury: Current status and future challenges. *Expert Rev. Neurother.* **11**, 1351–1353 (2011).
4. S. Harkema, Y. Gerasimenko, J. Hodes, J. Burdick, C. Angeli, Y. Chen, C. Ferreira, A. Willhite, E. Rejc, R. G. Grossman, V. Reggie Edgerton, Effect of epidural stimulation of the lumbosacral spinal cord on voluntary movement, standing, and assisted stepping after motor complete paraplegia: A case study. *Lancet* **377**, 1938–1947 (2011).
5. S. I. Park, D. S. Brenner, G. Shin, C. D. Morgan, B. A. Copits, H. U. Chung, M. Y. Pullen, K. N. Noh, S. Davidson, S. Ju Oh, J. Yoon, K.-I. Jang, V. K. Samineni, M. Norman, J. G. Grajales-Reyes, S. K. Vogt, S. S. Sundaram, K. M. Wilson, J. S. Ha, R. Xu, T. Pan, T.-i. Kim, Y. Huang, M. C. Montana, J. P. Golden, M. R. Bruchas, R. W. Gereau IV, J. A. Rogers, Soft, stretchable, fully implantable miniaturized optoelectronic systems for wireless optogenetics. *Nat. Biotechnol.* **33**, 1280–1286 (2015).
6. I. R. Minev, P. Musienko, A. Hirsch, Q. Barraud, N. Wenger, E. M. Moraud, J. Gandar, M. Capogrosso, T. Milekovic, L. Asboth, R. Fajardo Torres, N. Vachicouras, Q. Liu, N. Pavlova, S. Duis, A. Larmagnac, J. Vörös, S. Micera, Z. Suo, G. Courtine, S. P. Lacour, Electronic dura mater for long-term multimodal neural interfaces. *Science* **347**, 159–163 (2015).
7. A. F. Abouraddy, M. Bayindir, G. Benoit, S. D. Hart, K. Kuriki, N. Orf, O. Shapira, F. Sorin, B. Temelkuran, Y. Fink, Towards multimaterial multifunctional fibres that see, hear, sense and communicate. *Nat. Mater.* **6**, 336–347 (2007).
8. A. M. Stolyarov, L. Wei, F. Sorin, G. Lestoquoy, J. D. Joannopoulos, Y. Fink, Fabrication and characterization of fibers with built-in liquid crystal channels and electrodes for transverse incident-light modulation. *Appl. Phys. Lett.* **101**, 011108 (2012).
9. C. Lu, U. P. Froriep, R. A. Koppes, A. Canales, V. Caggiano, J. Selvidge, E. Bizzi, P. Anikeeva, Polymer fiber probes enable optical control of spinal cord and muscle function in vivo. *Adv. Funct. Mater.* **24**, 6594–6600 (2014).
10. A. Canales, X. Jia, U. P. Froriep, R. A. Koppes, C. M. Tringides, J. Selvidge, C. Lu, C. Hou, L. Wei, Y. Fink, P. Anikeeva, Multifunctional fibers for simultaneous optical, electrical and chemical interrogation of neural circuits in vivo. *Nat. Biotechnol.* **33**, 277–284 (2015).
11. M. Aden, A. Roesner, A. Olowinsky, Optical characterization of polycarbonate: Influence of additives on optical properties. *J. Polym. Sci. B* **48**, 451–455 (2010).
12. P. M. van Midwoud, A. Janse, M. T. Merema, G. M. Groothuis, E. Verpoorte, Comparison of biocompatibility and adsorption properties of different plastics for advanced microfluidic cell and tissue culture models. *Anal. Chem.* **84**, 3938–3944 (2012).
13. G. Khanarian, H. Celanese, Optical properties of cyclic olefin copolymers. *Opt. Eng.* **40**, 1024–1029 (2001).

14. B. Cortese, M. C. Mowlem, H. Morgan, Characterisation of an irreversible bonding process for COC–COC and COC–PDMS–COC sandwich structures and application to microvalves. *Sens. Actuators B* **160**, 1473–1480 (2011).
15. M. Quaglio, G. Canavese, E. Giuri, S. Luigi Marasso, Evaluation of different PDMS interconnection solutions for silicon, Pyrex and COC microfluidic chips. *J. Micromech. Microeng.* **18**, 055012 (2008).
16. L. Hu, H. S. Kim, J.-Y. Lee, P. Peumans, Y. Cui, Scalable coating and properties of transparent, flexible, silver nanowire electrodes. *ACS Nano* **4**, 2955–2963 (2010).
17. Z. Yu, Q. Zhang, L. Li, Q. Chen, X. Niu, J. Liu, Q. Pei, Highly flexible silver nanowire electrodes for shape-memory polymer light-emitting diodes. *Adv. Mater.* **23**, 664–668 (2011).
18. P. Lee, J. Lee, H. Lee, J. Yeo, S. Hong, K. H. Nam, D. Lee, S. S. Lee, S. H. Ko, Highly stretchable and highly conductive metal electrode by very long metal nanowire percolation network. *Adv. Mater.* **24**, 3326–3332 (2012).
19. S. P. Lacour, D. Chan, S. Wagner, T. Li, Z. Suo, Mechanisms of reversible stretchability of thin metal films on elastomeric substrates. *Appl. Phys. Lett.* **88**, 204103 (2006).
20. D. A. Chang-Yen, R. K. Eich, B. K. Gale, A monolithic PDMS waveguide system fabricated using soft-lithography techniques. *J. Lightwave Technol.* **23**, 2088–2093 (2005).
21. H. Ma, A. K.-Y. Jen, L. R. Dalton, Polymer-based optical waveguides: Materials, processing, and devices. *Adv. Mater.* **14**, 1339–1365 (2002).
22. H. Li, Y. Qi, J. P. Ryle, J. T. Sheridan, Self-written waveguides in a dry acrylamide/polyvinyl alcohol photopolymer material. *Appl. Opt.* **53**, 8086–8094 (2014).
23. B. Rubehn, S. B. Wolff, P. Tovote, A. Luthi, T. Stieglitz, A polymer-based neural microimplant for optogenetic applications: Design and first in vivo study. *Lab Chip* **13**, 579–588 (2013).
24. D. Snakenborg, G. Perozziello, H. Klank, O. Geschke, J. P. Kutter, Direct milling and casting of polymer-based optical waveguides for improved transparency in the visible range. *J. Micromech. Microeng.* **16**, 375 (2006).
25. S. Yun, S. Park, B. Park, Y. Kim, S. K. Park, S. Nam, K.-U. Kyung, Polymer-waveguide-based flexible tactile sensor array for dynamic response. *Adv. Mater.* **26**, 4474–4480 (2014).
26. M. Choi, J. W. Choi, S. Kim, S. Nizamoglu, S. K. Hahn, S. H. Yun, Light-guiding hydrogels for cell-based sensing and optogenetic synthesis in vivo. *Nat. Photonics* **7**, 987–994 (2013).
27. M. Choi, M. Humar, S. Kim, S. H. Yun, Step index optical fiber made of biocompatible hydrogels. *Adv. Mater.* **27**, 4081–4086 (2015).
28. A. Yildirim, M. Yunusa, F. E. Ozturk, M. Kanik, M. Bayindir, Surface textured polymer fibers for microfluidics. *Adv. Funct. Mater.* **24**, 4569–4576 (2014).
29. J. van de Groep, P. Spinelli, A. Polman, Transparent conducting silver nanowire networks. *Nano Lett.* **12**, 3138–3144 (2012).
30. E. Fiedler, N. Haas, T. Stieglitz, Suitability of SU-8, EpoClad and EpoCore for flexible waveguides on implantable neural probes, paper presented at the 36th Annual International Conference of the IEEE Engineering in Medicine and Biology Society (EMBC'2014), Chicago, IL, 26 to 30 August 2014.
31. M. Im, I.-J. Cho, F. Wu, K. D. Wise, E. Yoon, Neural probes integrated with optical mixer/splitter waveguides and multiple stimulation sites, paper presented at the IEEE 24th International Conference on Micro Electro Mechanical Systems (MEMS'2011), Cancun, 23 to 27 January 2011.
32. S. Royer, B. V. Zemelman, M. Barbic, A. Losonczy, G. Buzsáki, J. C. Magee, Multi-array silicon probes with integrated optical fibers: Light-assisted perturbation and recording of local neural circuits in the behaving animal. *Eur. J. Neurosci.* **31**, 2279–2291 (2010).
33. J. Wang, F. Wagner, D. A. Borton, J. Zhang, I. Ozden, R. D. Burwell, A. V. Nurmikko, R. van Wagenen, I. Diester, K. Deisseroth, Integrated device for combined optical neuromodulation and electrical recording for chronic in vivo applications. *J. Neural Eng.* **9**, 016001 (2012).
34. P. Anikeeva, A. S. Andalman, I. Witten, M. Warden, I. Goshen, L. Grosenick, L. A. Gunaydin, L. M. Frank, K. Deisseroth, Optetrode: A multichannel readout for optogenetic control in freely moving mice. *Nat. Neurosci.* **15**, 163–170 (2012).
35. J. Park, S. Choi, A. H. Janardhan, S.-Y. Lee, S. Raut, J. Soares, K. Shin, S. Yang, C. Lee, K.-W. Kang, H. R. Cho, S. J. Kim, P. Seo, W. Hyun, S. Jung, H.-J. Lee, N. Lee, S. H. Choi, M. Sacks, N. Lu, M. E. Josephson, T. Hyeon, D.-H. Kim, H. J. Hwang, Electromechanical cardioplasty using a wrapped elasto-conductive epicardial mesh. *Sci. Transl. Med.* **8**, 344ra386 (2016).
36. E. Kymakis, G. A. Amaratunga, Electrical properties of single-wall carbon nanotube-polymer composite films. *J. Appl. Phys.* **99**, 084302 (2006).
37. J. A. Rogers, T. Someya, Y. Huang, Materials and mechanics for stretchable electronics. *Science* **327**, 1603–1607 (2010).
38. D.-H. Kim, N. Lu, R. Ma, Y.-S. Kim, R.-H. Kim, S. Wang, J. Wu, S. M. Won, H. Tao, A. Islam, K. J. Yu, T.-i. Kim, R. Chowdhury, M. Ying, L. Xu, M. Li, H.-J. Chung, H. Keum, M. McCormick, P. Liu, Y.-W. Zhang, F. G. Omenetto, Y. Huang, T. Coleman, J. A. Rogers, Epidermal electronics. *Science* **333**, 838–843 (2011).
39. J. A. Fan, W.-H. Yeo, Y. Su, Y. Hattori, W. Lee, S.-Y. Jung, Y. Zhang, Z. Liu, H. Cheng, L. Falgout, M. Bajema, T. Coleman, D. Gregoire, R. J. Larsen, Y. Huang, J. A. Rogers, Fractal design concepts for stretchable electronics. *Nat. Commun.* **5**, 3266 (2014).
40. T. K. Kim, J. K. Kim, O. C. Jeong, Measurement of nonlinear mechanical properties of PDMS elastomer. *Microelectron. Eng.* **88**, 1982–1985 (2011).
41. E. C. Clarke, in *Neural Tissue Biomechanics* (Springer, 2011), pp. 25–40.
42. B. R. Arenkiel, J. Peca, I. G. Davison, C. Feliciano, K. Deisseroth, G. J. Augustine, M. D. Ehlers, G. Feng, In vivo light-induced activation of neural circuitry in transgenic mice expressing channelrhodopsin-2. *Neuron* **54**, 205–218 (2007).
43. L. A. Gunaydin, O. Yizhar, A. Berndt, V. S. Sohal, K. Deisseroth, P. Hegemann, Ultrafast optogenetic control. *Nat. Neurosci.* **13**, 387–392 (2010).
44. A. Prasad, M. Sahin, Chronic recordings from the rat spinal cord descending tracts with microwires, paper presented at the Annual International Conference of the IEEE Engineering in Medicine and Biology Society (EMBC'2011), Boston, MA, 30 August to 3 September 2011.
45. E. Azim, J. Jiang, B. Alstermark, T. M. Jessell, Skilled reaching relies on a V2a propriospinal internal copy circuit. *Nature* **508**, 357–363 (2014).
46. A. Tooker, V. Tolosa, K. G. Shah, H. Sheth, S. Felix, T. Delima, S. Pannu, Polymer neural interface with dual-sided electrodes for neural stimulation and recording, paper presented at the Annual International Conference of the IEEE Engineering in Medicine and Biology Society (EMBC'2012), San Diego, CA, 28 August to 1 September 2012.
47. T. Sainsbury, D. Fitzmaurice, Carbon-nanotube-templated and pseudorotaxane-formation-driven gold nanowire self-assembly. *Chem. Mater.* **16**, 2174–2179 (2004).
48. C. M. Gray, P. E. Maldonado, M. Wilson, B. McNaughton, Tetrodes markedly improve the reliability and yield of multiple single-unit isolation from multi-unit recordings in cat striate cortex. *J. Neurosci. Methods* **63**, 43–54 (1995).
49. T. Adrega, S. P. Lacour, Stretchable gold conductors embedded in PDMS and patterned by photolithography: Fabrication and electromechanical characterization. *J. Micromech. Microeng.* **20**, 055025 (2010).
50. E. Delivopoulos, D. J. Chew, I. R. Minev, J. W. Fawcett, S. P. Lacour, Concurrent recordings of bladder afferents from multiple nerves using a microfabricated PDMS microchannel electrode array. *Lab Chip* **12**, 2540–2551 (2012).


**Acknowledgments:** C.L. is grateful to M. J. Tarkanian and I. Feitler for their assistance with machining. **Funding:** This work was supported by the Center for Sensorimotor Neural Engineering, an NSF Engineering Research Center (EEC-1028725), NSF CAREER award to P.A. (CBET-1253890), NSF Center for Materials Science and Engineering (DMR-1419807, IRG-I), the National Institute of Neurological Disorders and Stroke (5R01NS086804), the U.S. Army Research Laboratory, and the U.S. Army Research Office through the Institute for Soldier Nanotechnologies (W911NF-13-D-0001). This work made use of facilities at the Center for Nanoscale Systems at Harvard University, which is a member of the NSF National Nanotechnology Infrastructure Network (ECS-0335765). S.P. is a recipient of Samsung Scholarship, and T.J.R. is a Washington Research Foundation Innovation Postdoctoral Fellow with the UW Institute of Neuroengineering. **Author contributions:** C.L. and P.A. designed the experiments. C.L., A.D., I.B., C.H., and S.R. fabricated and characterized fiber probes. C.L. performed mouse surgeries. C.L., S.P., T.J.R., and P.A. performed electrophysiological experiments and analyzed the data. C.L., S.P., J.K., and P.A. performed immunohistochemistry and analyzed the data. C.T.M. facilitated with the design of in vivo evaluation experiments. Y.F. aided with the design of fiber-based probes. All authors took part in the preparation of the manuscript. **Competing interests:** The authors declare that they have no competing interests. **Data and materials availability:** All data needed to evaluate the conclusions in the paper are present in the paper and/or the Supplementary Materials. Additional data may be requested from the authors. Physical samples of the fiber probes are available upon request.

Submitted 1 May 2016
Accepted 10 February 2017
Published 29 March 2017
10.1126/sciadv.1600955

**Citation:** C. Lu, S. Park, T. J. Richner, A. Derry, I. Brown, C. Hou, S. Rao, J. Kang, C. T. Moritz, Y. Fink, P. Anikeeva, Flexible and stretchable nanowire-coated fibers for optoelectronic probing of spinal cord circuits. *Sci. Adv.* **3**, e1600955 (2017).